OPTICAL RESPONSE OF COMPOSITE PLASMONIC STRUCTURES

N. Mitetelo [a], S. Svyakhovskiy [a], A. Gartman [a], A. Tepanov [b], and A. Maydykovskiy [a]

[a] *Department of Physics, M. V. Lomonosov Moscow State University, Leninskiye Gory 1–2, 119991 Moscow, Russia*
[b] *Department of Chemistry, M. V. Lomonosov Moscow State University, Leninskiye Gory 1–3, 119991 Moscow, Russia*
E-mail: nickm@shg.ru

Here we demonstrate the composition of a 3D porous quartz matrix infiltrated by silver nanoparticles as a possible application for surface enhanced Raman scattering (SERS) investigations. Various types of infiltration techniques applied for the incorporation of plasmonic Ag nanoparticles inside the pores are considered. We observe an enhancement of the second harmonic generation intensity, two-photon luminescence and nonlinear absorption in the composite metal–dielectric structures in the spectral vicinity of the localized surface plasmon resonance in silver nanoparticles, which confirms the related amplification of the local field effects in these 3D composite structures.

Keywords: plasmon resonance, second harmonic generation, local field, porous quartz, silver nanoparticles

PACS: 81.05.Rm, 81.05.Zx, 82.45.Aa, 87.64.kp, 42.70.Ce

1. Introduction

The optical and nonlinear-optical response of various types of structures containing plasmonic metallic nanoparticles has been the subject of intensive studies over the last decades [1]. The main goal here is the search for an optimal design providing the amplification of the local optical fields in such structures and thus of the efficiency of the light–matter interaction, which is important, first of all, for sensors. Thus an amplification of the Raman signal of about 10^6 times has been already reported [2], and even up to 10^{11} [3]. Most of the studies were performed for planar structures coated by metallic nanoparticles or for nanostructured metallic films [4], while the application of three-dimensional structures seems much more promising due to a larger (internal) surface area. If this surface is made functional, i.e. enhances the optical field close to it, this should lead to a manifold increase of the interaction between the structure and the incident wave. As an example, an effective enhancement of the surface enhanced Raman scattering (SERS) in nanoparticle-functionalized porous polymers and in ZnO nanorods coated by silver nanoparticles was shown in [5].

An important characteristic of metallic nanostructures for the amplification of the local optical fields is the presence of the localized plasmon resonance that may be visualized by an absorption peak, which is typically observed close to 570 nm wavelength in the case of gold nanoparticles (NPs) and to 400 nm in the case of silver NPs, these resonant wavelengths being dependent on the optical properties of the matrix. Local field effects can be studied by using the nonlinear optical methods due to their nonlinear dependence on the local field strength.

For spectroscopy applications, the requirement for the 3D enhancing substrates is their optical transparency (low absorption). In this aspect, the structures based on transparent porous quartz as a matrix for the metallic nanoparticles have distinct advantages in comparison to other structures, which usually have higher optical losses. To the best of our knowledge, there have been no studies on the composite structures based on porous quartz with silver nanoparticles.

In this work we describe the results of experimental studies of composite plasmonic structures based on porous quartz with silver nanoparticles on its walls prepared by different methods. Processes of fabrication and optical investigation are

described, and also parameters which provide the biggest enhancement of the linear and nonlinear response are brought out.

2. Fabrication of metal–dielectric composite films

Porous quartz films used as a dielectric matrix for further infiltration by silver nanoparticles (NPs) were made in several steps. First, a film of porous silicon of 200 μm thick is made by electrochemical etching of silicon with crystallographic orientation (001) in a 27% hydrofluoric acid solution similarly to the method described in [6], the average diameter of the pores being about 50 nm. In the second step, the porous silicon film was annealed in the air atmosphere at the temperature of about 750 °C for 10 hours, so that the porous silicon was totally oxidized and transformed to porous silica. Figure 1(a) shows a typical scanning
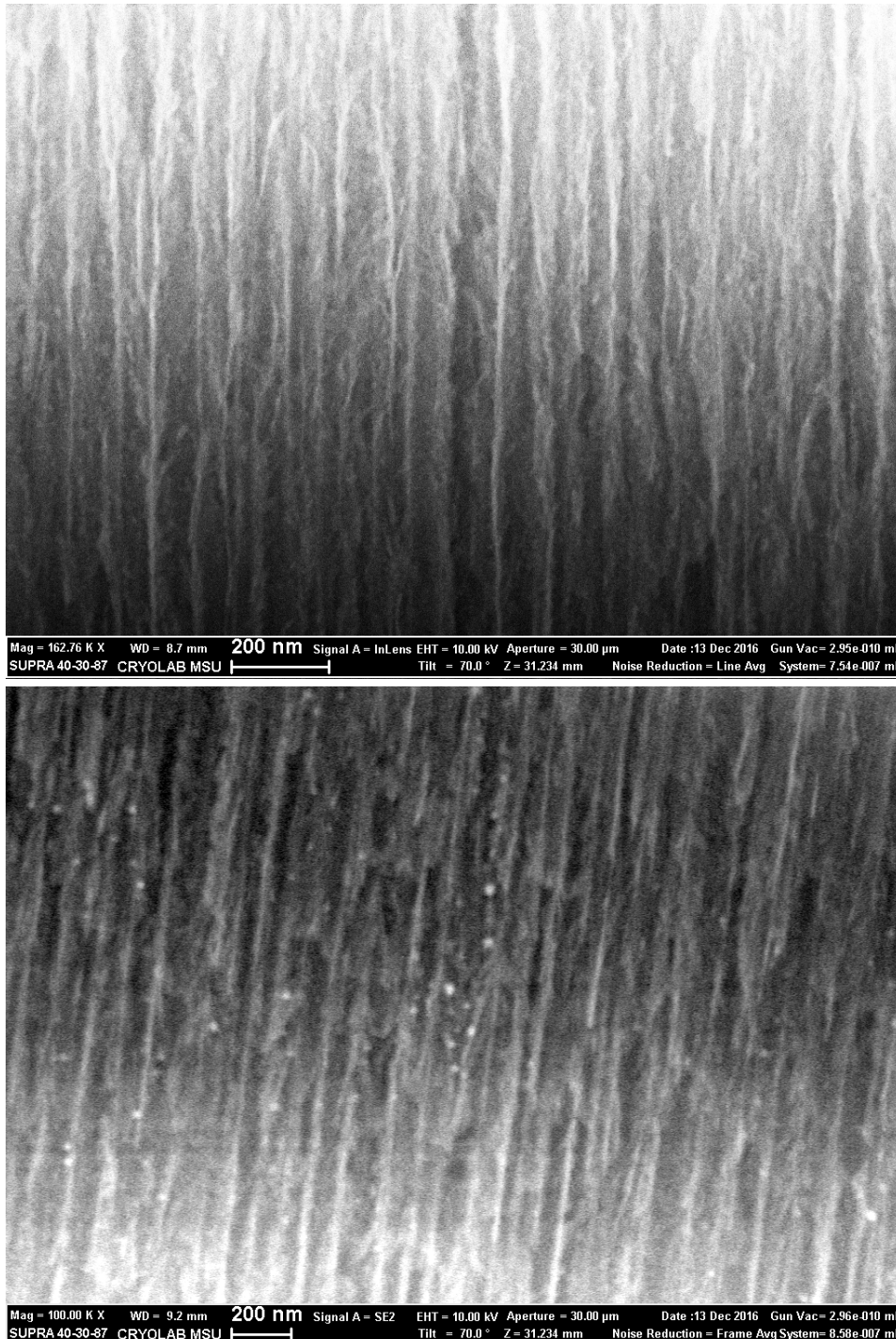

Fig. 1. Scanning electron microscopy images of the cross-section of (a) a porous quartz film and (b) such a film infiltrated by Ag nanoparticles, which appear as bright white points on the image. Average NPs volume density equals approximately $2.5 \cdot 10^{14}$ cm^{-3}.

electron microscopy (SEM) image of the cross-section of a porous quartz film. The surface area of pores in the composed porous silica films estimated by the nitrogen-adsorption method [7] was approximately 200 m^2/g.

For the infiltration of porous silica films by silver NPs we used three technological approaches:

(1) Vacuum infusion of an aqueous solution of Ag NPs of the mass concentration of 500 μg/ml, the Ag NPs sizes being about 10±5 nm. Figure 2 shows a NPs size bar chart. Silver nanoparticles in a liquid solution were made by the chemical reduction of $AgNO_3$ by sodium borohydride. In order to provide the aggregate stability, polyhexamethylene biguanide (PHMB) was used during the formation of nanoparticles. For the infiltration, a porous silica film was placed in the liquid solution of nanoparticles, which was set in a vacuum chamber (residual pressure of 0.01 bar) with the possibility to pump out air from the pores. After several infiltration series nothing prevents the liquid solution from filling the pores. The SEM image of the infiltrated porous silica is shown in Fig. 1(b).

(2) Thermal reduction of silver nanoparticles from $AgNO_3$ nanocrystals embedded in the porous silica template [8]. In this method, a drop of an aqueous solution of 0.5 M $AgNO_3$ was put on the surface of a flat porous silica film, over an area of approximately 0.5 cm^2. Drying off the solvent leads to the formation of $AgNO_3$ nanocrystals inside the pores. Thermal reduction of the crystallites was performed by thermal annealing in ambient atmosphere at 450 °C, which results in the formation of a composite structure. It is worth noting that this technique can be successively applied for the infiltration of a porous structure by the required concentration of Ag, while a relatively wide distribution in nanoparticle sizes was obtained. But the quality of the NP surface prepared by this method was not smooth enough for nonlinear investigations where better quality is needed.

(3) Supercritical fluid impregnation in an aqueous carbon-dioxide solution of Ag NPs [9] at the pressure of approximately 200 bars, followed by further photoreduction of silver from a precursor under a continuous laser irradiation at 405 nm wavelength.

It is necessary to mention that all these methods give a possibility to distribute nanoparticles in the bulk of a porous structure, while the third technique needs to be improved in order to increase the volume concentration of the nanoparticles, as the latter was less than approximately one nanoparticle per 10 pores. At the same time, the filling density of NPs provided by the first and the second methods can be made quite large. Still all three techniques demonstrate a successive incorporation of metallic nanoparticles into porous matrixes.

One more important parameter of the metal–dielectric composites is the quality of the metallic nanoparticles, which can be different for each
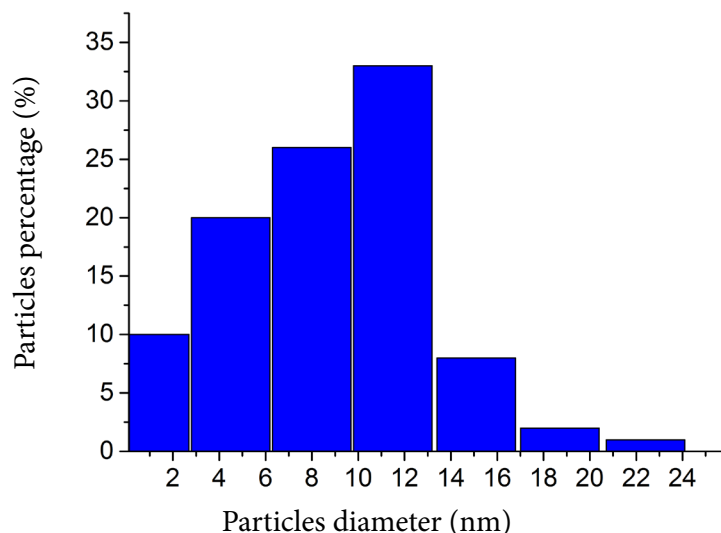

Fig. 2. Size distribution of silver nanoparticles in an aqueous solution of Ag(PHMB).

kind of the fabrication technique. As it is discussed below, we consider the first method of the vacuum infusion of Ag NPs as the best candidate for the composition of plasmonic metal–dielectric composites.

3. Optical studies of composite plasmonic structures

For the characterization of the Ag NPs plasmonic properties, the optical density spectra of the aqueous solutions of different concentrations of Ag NPs were measured. Figure 3 shows the spectral dependences of aqueous solutions of the Ag nanoparticles placed in a cuvette of 10 mm in length in a Lambda 25 spectrophotometer (*PerkinElmer*). It can be seen that the absorption spectra shift to larger wavelengths with increasing concentration of metal nanoparticles and their diameter. This may be due to two possible reasons, namely, to an increase of the interparticle interaction, or a coalescence of the Ag NPs. In accordance with the theoretical predictions, both effects should experience a redshift. One can also mention an increase of the full width at half maximum (FWHM) when the NPs concentration is increased, which can be also consistent with the same two effects.

Figure 4 shows the extinction spectra of an aqueous liquid solution of Ag(PHMB) and of a porous film (thickness was approximately 20 μm) with embedded nanoparticles and composed by the vacuum infusion (1st method). In both cases

there are absorption peaks at the wavelength of approximately 420 nm, which refer to the excitation of the localized plasmon resonance in the nanoparticles.

These porous matrices were characterized by linear spectroscopy methods, which allowed us to estimate the concentration of nanoparticles in the porous structure as $2.5 \cdot 10^{14}$ cm^{-3}. This value is larger than for a liquid solution. The spectral position of the peak absorption wavelength λ_{max} for a composite consisting of core–shell metal nanoparticles in a dielectric matric is given by [10]

$$\lambda_{max} = \lambda_p [\varepsilon_{ib} + \frac{3}{f}(\varepsilon_m + \frac{\varepsilon_c}{2})]^{1/2}, \tag{1}$$

where λ_p is the wavelength of the electron plasma oscillations in bulky metal, ε_m is the dielectric permittivity of metal, ε_{ib} is the permittivity describing the electron transitions in the matrix material, ε_c is the core material permittivity, f is the volume fraction of metal in the nanoparticle with the shell. Such a model can be used in our case as, in fact, we used core–shell nanoparticles for the infiltration of the porous matrices, the core being an Ag nanoparticle and the shell being a surface-active stabilizing substance such as PHMB.

We show as well a way for the control over the efficiency of the plasmon resonance excitation and its spectrum by using the agglomeration of Ag NPS induced by the presence of KCl in a NPs solution, which decreases the aggregate stability
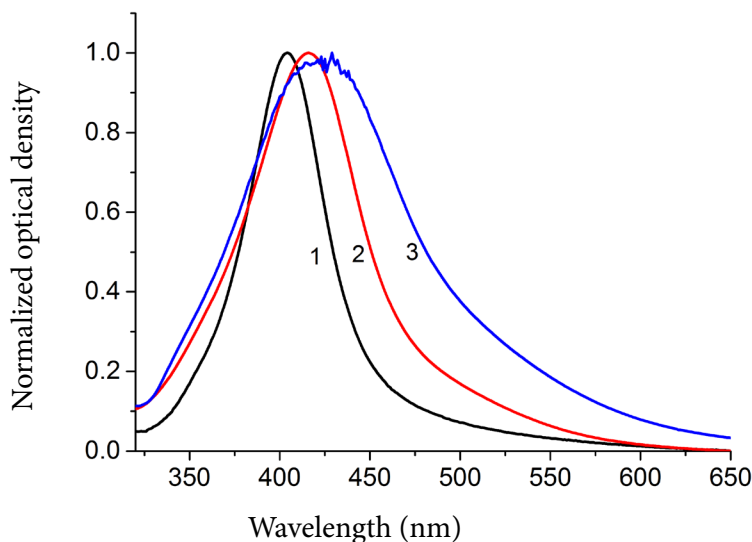

Fig. 3. Normalized optical density spectra of silver NPs in an aqueous liquid solution of the mass density: (1) 50 μg/ml (black), (2) 500 μg/ml (red online), and (3) 1000 μg/ml (blue online). 1 corresponds to 8±3 nm nanoparticle diameter, (2) is 10±5 nm, (3) is 15±6 nm.

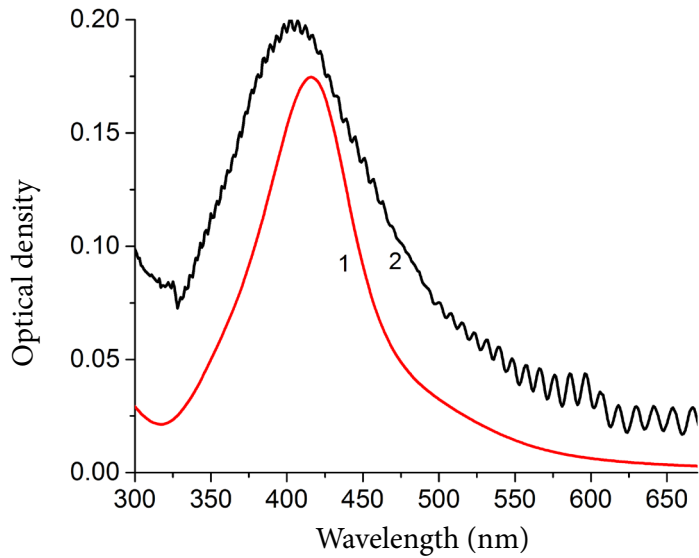Fig. 4. Absorption spectra of Ag(PHMB) nanoparticles in a liquid solution (1) and incorporated into the porous quartz film (20 μm) infiltrated by vacuum infusion method (2) with the same NPs. Blue shift corresponds to the NPs surrounding modification.

of NPs. Thus the diameter of the Ag particles aggregates should increase when the KCl concentration rises. Figure 5 shows that increasing of nanoparticle's diameter due to this subjection leads to the red shift ($\lambda_{max} \sim d^2$ as predicted in [10]) in the absorption spectrum and its broadening [11].

Nonlinear-optical studies were performed for the composite structures made by all three composition methods using the second harmonic generation (SHG) spectroscopy technique [12]. In this experiment the fundamental wavelength of a Ti-sapphire laser with the 80 fs pulse duration tunable in the wavelength range 720–890 nm was used as the fundamental radiation, that was fo-

cused on the sample into a spot of approximately 36 μm in diameter. The peak intensity in the focus of the lens used in this experiment was approximately 100 MW/cm². The spectrum of the intensity of the nonlinear optical response of a 3D composite porous film is shown in Fig. 6, the left panel. It can be seen that the scattered radiation has two spectral components: the first refers to the second harmonic of the 880 nm fundamental wavelength and the second is a broad peak of two-photon luminescence (TPL) in the region of 460–560 nm. The latter should be attributed to the presence of an organic core covering the Ag NPs. The pump-wavelength for nonlinear investigations was
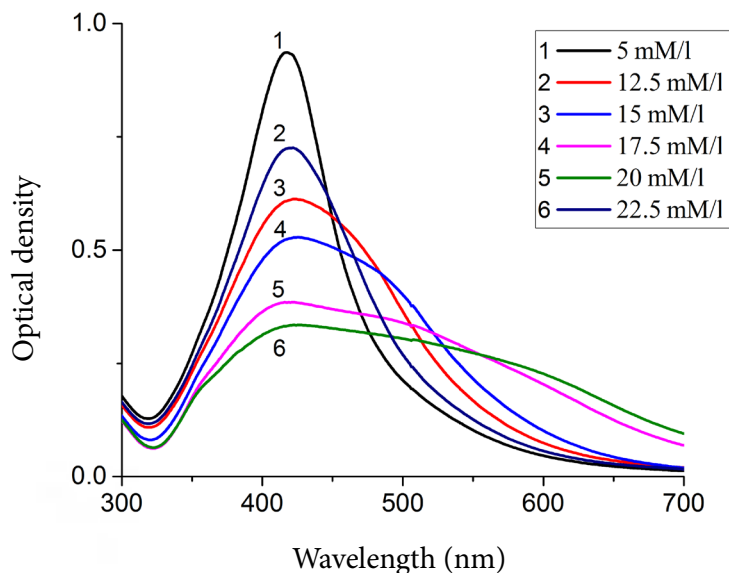

Fig. 5. Spectral dependences of the optical density of a liquid solution of 500 μg/ml Ag(PHMB) nanoparticles with different concentration of KCl (from 5 to 22.5 mM/l).
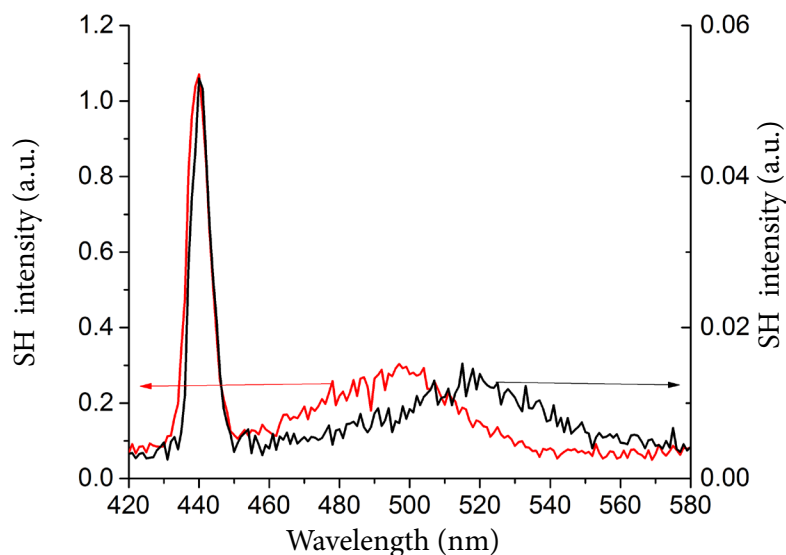
Fig. 6. Spectral dependences of the nonlinear response of 3D and 2D samples containing Ag NPs for the fundamental wavelength of 880 nm. Strong maxima at 440 nm reveal the SH generation, broad maxima centered around 500 nm correspond to the two-photon excited luminescence of NPs.

chosen at 880 nm for its corresponding with the thick 200 μm composite sample's spectral position of the absorption peak.

For comparison, we measured the nonlinear spectrum of a reference 2D plasmonic structure of the same Ag NPs placed as an array on a quartz plate. The quartz surface was activated by a 0.1% 3-APTES solution in order to prevent the formation of Ag NPs conglomerates. The SEM image of the 2D structure is shown in Fig. 7, which proves that the nanoparticles are uniformly distributed over the surface without forming conglomerates. The nonlinear optical spectrum of the 2D array of Ag NPs is shown in Fig. 6, the right panel. It reveals similar spectral features as in the case of the 3D composite porous quartz film, while the intensity of the registered signal is at least 20 times smaller for the 2D structure.

It is worth noting that for the 740 nm wavelength of the fundamental radiation, i.e. as the second harmonic is relatively far from the peak of the plasmonic resonance region, the SHG
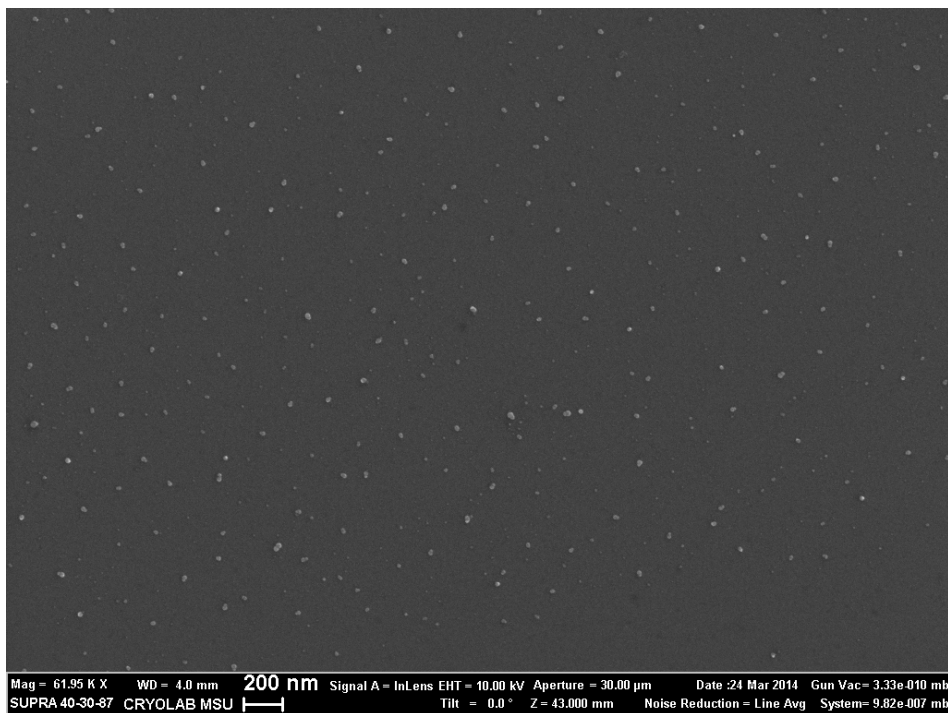

Fig. 7. Scanning electron microscopy image of a planar quartz structure with Ag nanoparticles.

intensity is much smaller, which indicates a clear plasmon-assisted amplification of the nonlinear response. When the plasmon resonance is achieved at the second harmonic wavelength, the SHG intensity $I(2\omega)$ can be described by the expression

$$I(2\omega) \sim |\chi^{(2)}|^2 |L(\omega)|^4 |L'(2\omega)|^2 |E(\omega)|^4, \tag{2}$$

where $L'(2\omega)$ is the local field factor of a medium at the SHG wavelength. In the simplest case of a spherical nanoparticle the local field factor is $L'(2\omega) = \dfrac{3}{\varepsilon(2\omega)+2}$.

In order to characterize the nature of the nonlinear-optical response of the 3D composite porous quarts film with Ag NPs, we studied the angular distribution of the intensity of the nonlinear-optical signal, i.e. the SHG and TPL intensity. The corresponding scattering is indicated in Fig. 8. As shown in [13], it contains information on the correlation length of the nonlinear sources, l_{corr}, in accordance with the following expression:

$$I(\theta) \sim \exp\left(\frac{2\pi l_{corr}}{\lambda_{NLO}} \sin\theta\right). \tag{3}$$

Here I is the measured intensity, θ is the scattering angle counted from the direction of the film transmitted through the composite film, λ_{NLO} is the wavelength of the nonlinear signal. The approximation of the experimental data by Eq. (3) gives the value $l_{corr} = 100$ nm for the 3D-sample. For the considered composite porous quartz structures this length should be associated with the average in-plane distance between the Ag nanoparticles.

4. Nonlinear absorption studies

The third-order nonlinear effect of two-photon absorption was also studied in order to characterize the local field effects in the composites, which was expected to be high as the samples reveal the surface plasmon resonance at the doubled frequency of the fundamental beam. One of the most effective methods of studying this effect is the Z-scan technique [15] developed by Sheik-Bahae and coworkers. Here the normalized transmission is measured as a function of the incident field intensity, which is varied by moving the sample with the thickness L along the z axis of the lens. The nonlinear absorption described by the coefficient β becomes important closer to the lens focal plane $z = 0$, where the laser beam intensity is high, so the total absorption coefficient α is described by the expression

$$\alpha = \alpha_0 + \beta I_0, \tag{4}$$

where I_0 is the laser beam intensity just after the focusing lens. Typically the coordinate z is measured in units of the Rayleigh length z_0 and is given by

$$T(z) \sim 1 - \frac{\beta L_{eff} I_0}{1 + (z/z_0)}, \quad L_{eff} = \frac{1 - e^{-\alpha L}}{L}. \tag{5}$$
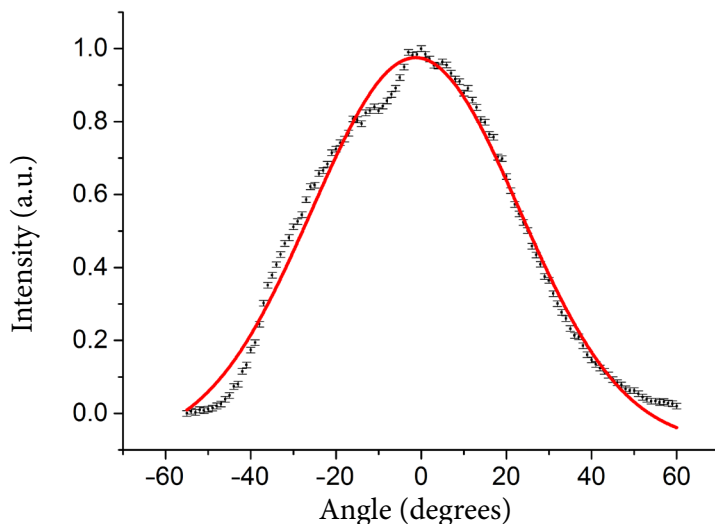

Fig. 8. Scattering diagram of the intensity of the nonlinear optical signal (SHG+TPL) measured versus the polar angle in transmission through the composite 3D porous quartz infiltrated by Ag NPs. Fundamental beam at 880 nm is directed along the normal to the surface of the composite structure; zero scattering angle corresponds to the direction of the transmitted beam. Solid line is the result of the approximation by Eq. (3).

The results of the Z-scan dependences obtained for the sample that was used in the nonlinear measurements described above are shown in Fig. 9. The value of the two-photon absorption coefficient estimated from the Z-scan curve 1 is quite large: $\beta = 1.2 \cdot 10^{-6}$ cm/W. This is larger as compared with the typical β values of the third-order nonlinear crystals.

Curves 2 and 3 in Fig. 9 demonstrate that the saturable absorption becomes the most pronounced effect at the laser intensities above $I_0 = 15$ MW/cm². It appears as an increase of the normalized transmittance at $z \to 0$. It can be seen that the saturable absorption overcomes the nonlinear absorption for $I_0 = 20$ MW/cm², as no minimum is observed at the $z = 0$ position of the sample.

Taking into account the obtained data, one can say that an enhancement of the Stokes-component in surface-enhanced Raman scattering can be of about 400, due to a 20-fold enhancement of the SHG intensity in our 3D structures, as

$$F \sim \eta |L(\omega)|^4 |E(\omega)|^2, \tag{6}$$

where F is the Raman scattering (or fluorescence) intensity, $L(\omega)$ is the local field factor and $I(2\omega)$ is obtained by Eq. (2). In the case of SHG $|L'(2\omega)|^2$ is enhanced and the Stokes-component's signal is proportional to $|L(\omega)|^4$. So, if frequencies corresponding to these local field factors are both located in the plasmon enhancement region, we can obtain the enhancement of SHG and Raman-scattering.

4. Conclusions

Summing up, we discuss the ways for the composition of 3D metal–dielectric porous matrices exhibiting plasmon resonance excitation. The samples composed by vacuum infusion of Ag nanoparticles and those where the NPs are made by thermal and laser reduction of silver are demonstrated, all of them revealing an absorption maximum at the wavelength of 420 nm associated with plasmon excitation in Ag NPs. It is shown that the absorption spectrum is sensitive to the size distribution of NPs in a dielectric matrix. Local field effects in the composed 3D structures are revealed by nonlinear optical measurements of the second harmonic generation and nonlinear absorption, that show a substantial increase as compared to a 2D array of Ag NPs. We also demonstrate that saturable absorption in 3D metal–dielectric films is attained at relatively low values of the intensity of the fundamental beam of 15 mW/cm² in the vicinity of the two-photon plasmon resonance.
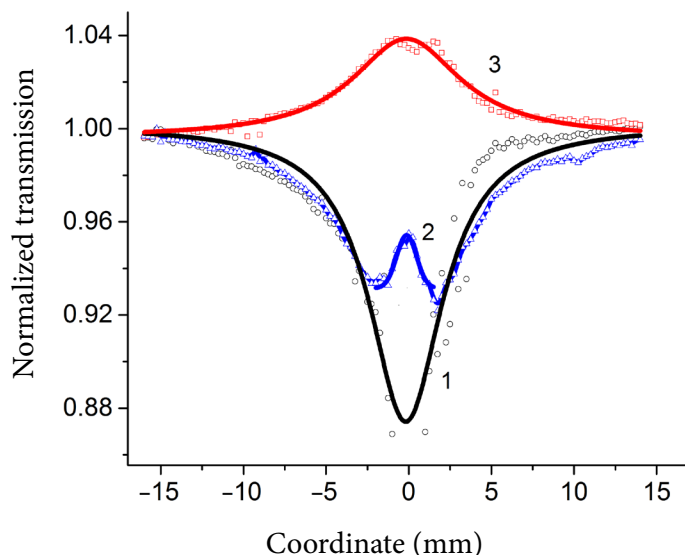
Fig. 9. Z-scan dependences (normalized transmission vs the coordinate of the translator, z) of a composite structure made of a porous quartz film with Ag NPs measured for the values of the input intensity $I_0 = 6$ MW/cm² (black), $I_0 = 15$ MW/cm² (blue online), and $I_0 = 24$ MW/cm² (red online). Experimental data (symbols) and approximation by Eq. (5).

References

[1] W.Q. Lim and Z. Gao, Plasmonic nanoparticles in biomedicine, Nano Today **11**(2), 168–188 (2016).

[2] J.F. Li, Y.J. Zhang, and S.Y. Ding, Core–shell nanoparticle-enhanced Raman spectroscopy, Chem. Rev. **117**(7), 5002–5069 (2017).

[3] E.J. Blackie, E.C.L. Ru, and P.G. Etchegoin, Single-molecule surface-enhanced Raman spectroscopy of nonresonant molecules, J. Am. Chem. Soc. **131**(40), 14466–14472 (2009).

[4] S. Bai, W. Zhou, Y. Lin, Y. Zhao, T. Chen, A. Hu, and W.W. Duley, Ultraviolet pulsed laser interference lithography and application of periodic structured Ag-nanoparticle films for surface-enhanced Raman spectroscopy, J. Nanopart. Res. **16**(7), 2470 (2014).

[5] O. Lupan, V. Cretu, V. Postica, M. Ahmadi, B.R. Cuenya, L. Chow, and R. Adelung, Silver-doped zinc oxide single nanowire multifunctional nanosensor with a significant enhancement in response, Sensor. Actuator. B **223**, 893–903 (2016).

[6] H. Robbins and B. Schwartz, Chemical etching of silicon, J. Electrochem. Soc. **106**(6), 505–508 (1959).

[7] G. Wang, K. Wang, and T. Ren, Improved analytic methods for coal surface area and pore size distribution determination using 77 K nitrogen adsorption experiment, Int. J. Min. Sci. Technol. **24**(3), 329–334 (2014).

[8] Y. Sun, B. Mayers, and Y. Xia, Transformation of silver nanospheres into nanobelts and triangular nanoplates through a thermal process, Nano Lett. **3**(5), 675–679 (2003).

[9] V. Arakcheev, V. Bagratashvili, A. Bekin, D. Khmelenin, N. Minaev, V. Morozov, and A. Rybaltovsky, Laser assisted synthesis of silver nanoparticles in silica aerogel by supercritical deposition technique, J. Supercrit. Fluids (2017).

[10] B.N. Khlebtsov and N.G. Khlebtsov, Multipole plasmons in metal nanorods: scaling properties and dependence on particle size, shape, orientation, and dielectric environment, J. Phys. Chem. C **111**(31), 11516–11527 (2007).

[11] V.A. Markel and V.A. Shalaev, Small-particle composites. I. Linear optical properties, Phys. Rev. B **53**(5), 2425 (1996).

[12] T.V. Murzina, T.V. Misuryaev, A.F. Kravets, J. Güdde, D. Schuhmacher, G. Marowsky, and O.A. Aktsipetrov, Nonlinear magneto-optical Kerr effect and plasmon-assisted SHG in magnetic nanomaterials exhibiting giant magnetoresistance, Surf. Sci. **482**, 1101–1106 (2001).

[13] E.D. Mishina, T.V. Misuryaev, A.A. Nikulin, V.R. Novak, T. Rasing, and O.A. Aktsipetrov, Hyper-Rayleigh scattering from Langmuir films of C 60 and its derivatives, J. Opt. Soc. Am. B **16**(10), 1692–1696 (1999).

[14] O.A. Aktsipetrov, Giant nonlinear optical effects on metal surfaces, Soros Scientific Journal, 109–116 (2007).

[15] M. Sheik-Bahae, A.A. Said, T.H. Wei, D.J. Hagan, and E.W. van Stryland, Sensitive measurement of optical nonlinearities using a single beam, IEEE J. Quantum Electron. **26**(4), 760–769 (1990).

KOMPOZITINIŲ PLAZMONINIŲ DARINIŲ OPTINIS ATSAKAS

N. Mitetelo [a], S. Svyakhovskiy [a], A. Gartman [a], A. Tepanov [b], A. Maydykovskiy [a]

[a] *Maskvos valstybinio M. Lomonosovo universiteto Fizikos fakultetas, Maskva, Rusija*
[b] *Maskvos valstybinio M. Lomonosovo universiteto Chemijos fakultetas, Maskva, Rusija*